



Interpolating between Soft and Hard Dynamics in Deep Inelastic Scattering .

P. Desgrolard, L. Jenkovszky, F. Paccanoni

► To cite this version:

P. Desgrolard, L. Jenkovszky, F. Paccanoni. Interpolating between Soft and Hard Dynamics in Deep Inelastic Scattering .. European Physical Journal C: Particles and Fields, 1999, 7, pp.263-270. 10.1007/s100520050405 . in2p3-00000214

HAL Id: in2p3-00000214

<https://hal.in2p3.fr/in2p3-00000214>

Submitted on 25 Feb 1999

HAL is a multi-disciplinary open access archive for the deposit and dissemination of scientific research documents, whether they are published or not. The documents may come from teaching and research institutions in France or abroad, or from public or private research centers.

L'archive ouverte pluridisciplinaire **HAL**, est destinée au dépôt et à la diffusion de documents scientifiques de niveau recherche, publiés ou non, émanant des établissements d'enseignement et de recherche français ou étrangers, des laboratoires publics ou privés.

INTERPOLATING BETWEEN SOFT AND HARD DYNAMICS IN DEEP INELASTIC SCATTERING

P. Desgrolard ⁽¹⁾, L. Jenkovszky ⁽²⁾, F. Paccanoni ⁽³⁾

⁽¹⁾ *Institut de Physique Nucléaire de Lyon, IN2P3-CNRS et Université Claude Bernard, F69622 Villeurbanne Cedex, France.*

⁽²⁾ *Bogolyubov Institute for Theoretical Physics, Kiev-143, Ukraine.*

⁽³⁾ *Dipartimento di Fisica, Università di Padova, Istituto Nazionale di Fisica Nucleare, Sezione di Padova, via F.Marzolo, I-35131 Padova, Italy.*

Abstract

An explicit model for the proton structure function is suggested, interpolating between low- Q^2 vector meson dominance and Regge behavior, on the one hand, and the high- Q^2 solution of the Gribov-Lipatov-Altarelli-Parisi evolution equation, on the other hand. The model is fitted to the experimental data in a wide range of the kinematical variables with emphasis on the low- x HERA data. The boundaries, transition region and interface between various regimes are quantified.

¹E-mail: desgrolard@ipnl.in2p3.fr

²E-mail: jenk@gluk.apc.org

³E-mail: paccanoni@pd.infn.it

1 INTRODUCTION

In deep inelastic scattering the dynamics of low - and high virtualities, Q^2 is usually treated in a disconnected way, by using different methods. The structure function (SF) $F_2(x, Q^2)$ at small Q^2 (and small x , where x is the fraction of the momentum carried by a parton) is known to be Regge-behaved and satisfying vector meson dominance (VMD) with the limit $F_2(x, Q^2) \xrightarrow{Q^2 \rightarrow 0} 0$, imposed by gauge invariance. At large Q^2 , on the other hand, $F_2(x, Q^2)$ obeys the solutions of the Gribov-Lipatov-Altarelli-Parisi (GLAP) evolution equation [1].

One important problem remains open: where do these two regimes meet and how do they interpolate? In the present paper we seek answers to these questions.

For definiteness, we deal with the proton SF to be denoted F_2 . Our emphasis is on the small x region, dominated by gluodynamics. The valence quark contribution will be added at large- x in a phenomenological way to make the fits complete.

The forthcoming presentation has also an important aspect relevant to quantum chromodynamics (QCD), namely in clarifying the range of applicability and the interface between the GLAP and the Balitsky-Fadin-Kuraev-Lipatov (BFKL) [2] evolutions. While the GLAP equation describes the evolution of the SF in Q^2 starting from a given x -dependence, the BFKL evolution means variation of the SF in x for fixed Q^2 , both implying large enough Q^2 for the perturbative expansion to be valid. QCD leaves flexible the relevant limits and boundaries. Moreover, the onset of their asymptotic solutions depends on details of the calculations. In this paper we try to make some of these limits explicit and quantitative.

HERA is an ideal tool to verify the above theories. The relevant data extend over a wide range of Q^2 - a fruitful test field for the GLAP evolution, on one hand, and to low enough x , where the SF is dominated by a Pomeron contribution, expected to be described by the BFKL evolution (see below).

For the parametrization $F_2 \approx x^\lambda$, the "effective power" λ rises on average from about 0.15 around $Q^2 \approx 1 \text{ GeV}^2$ to 0.4 at $Q^2 \approx 1000 \text{ GeV}^2$ [3]. This exponent cannot be identified with the intercept - 1 of a simple Pomeron pole since by factorization it cannot depend on the virtuality of the external particle. A Q^2 -dependent intercept, compatible with the data, may arise from unitarization. However such a model [4] leaves much flexibility since neither the input (Born) value of the intercept is known for sure, nor a reliable unitarization procedure exists (for a recent attempt see however [5]). Moreover, claims exist that the HERA data are compatible with a softer, namely logarithmic behavior in x (obeying the Froissart bound) with a factorized Q^2 dependence [6, 7].

On the other hand the Q^2 , or GLAP, evolution in the "leading-log" approximation, has the following asymptotic solution for the singlet SF, valid for low x and high Q^2 [1, 8]

$$F_2 \approx \sqrt{\gamma_1 \ln(1/x) \ln \ln Q^2}, \quad (1.1)$$

with $\gamma_1 = \frac{16N_c}{(11-2f/3)}$. For 4 flavours ($f = 4$) and three colours ($N_c = 3$), one gets $\gamma_1 = 5.76$.

The asymptotic solution of the BFKL evolution equation is the so-called "Lipatov Pomeron" [2]. The numerical value of its intercept was calculated [2] to be between 1.3 and 1.5. This large value gave rise to speculations that the "Lipatov Pomeron" has been seen at HERA, where the large - Q^2 data seemed to be compatible with a steep rise $\approx x^{-0.4}$ (for an alternative interpretation of the relation between the "Lipatov Pomeron" and the "HERA effect" see for example [9]). However, according to the results of a recent calculation [10], the sub-asymptotic corrections to the Pomeron pole in perturbative QCD are larger than expected and they con-

tribute destructively to the intercept, thus lowering its value and making it compatible with the intercept of the soft Pomeron ⁴.

The technical difficulties of the purely perturbative calculations are aggravated by the unpredictable non-perturbative contributions, both in the BFKL and GLAP evolutions, thus reducing the precision of the theoretical calculations and their predictive power. All these difficulties are redoubled by the unknown unitarity corrections to be included in the final result.

Attempts to extrapolate the Pomeron-dominated "soft" SF by applying GLAP evolution towards higher Q^2 are known in the literature (see *e.g.* [4, 11]). They differ in some details, namely in the choice of the model for the Pomeron, its range, *i.e.* the value of Q^2 from which the evolution starts, and in the details of the evaluation (explicit in [11] or numerical in [4a]) of this evolution. We are not aware of any results of an "inverse extrapolation".

The situation has been recently summarized [3] in a figure (see also Sec. 6) showing the x - and Q^2 - dependence of the derivative $dF_2/d\ln Q^2$. The philosophy behind this figure is that the turning point (located at $Q^2 \sim 2 \text{ GeV}^2$) divides "soft" and "hard" dynamics. As shown in [3], one of the most successful approaches to the GLAP evolution, that by Ref. [12], fails to follow the soft dynamics. A phenomenological model (called "ALLM") for the structure function and cross-section, applicable in a wide range of their kinematical variables is well known in the literature [13]. Recently [14] it was updated to fit the data and shown to exhibit both - the rising and falling - parts of the derivative versus x (or Q^2). We will comment more the behavior of this derivative in Sec. 6.

Below we pursue a pragmatic approach to the problem. We seek for an interpolation formula between the known asymptotic solutions imposed as boundary conditions. Clearly, such an interpolation is not unique, but it seems to be among the simplest. Moreover, it fits the data remarkably well, thus indicating that the interpolation is not far from reality.

2 KINEMATICS

We use the standard kinematic variables to describe deep inelastic scattering:

$$e(k) + p(P) \rightarrow e(k') + X, \quad (2.1)$$

where k, k', P are the four-momenta of the incident electron, scattered electron and incident proton. Q^2 is the negative squared four-momentum transfer carried by the virtual exchanged boson (photon)

$$Q^2 = -q^2 = -(k - k')^2, \quad (2.2)$$

x is the Björken variable

$$x = \frac{Q^2}{2P \cdot q}, \quad (2.3)$$

y (the inelasticity parameter) describes the energy transfer to the final hadronic state

$$y = \frac{q \cdot P}{k \cdot P}, \quad (2.4)$$

W is the center of mass energy of the $\gamma^* p$ system

$$W^2 = Q^2 \frac{1-x}{x} + m_p^2, \quad (2.5)$$

⁴One of us (F.P.) thanks B.I. Ermolaev for a discussion of this issue.

with m_p , being the proton mass. Note that only two of these variables are independent and that, at high energies for a virtual photon with $x \ll 1$, one has $W^2 \sim \frac{Q^2}{x}$.

3 STRUCTURE FUNCTION FOR SMALL x AND ALL Q^2

Following the strategy outlined in the Introduction, we suggest the following ansatz for the small- x singlet part (labelled by the upper index $S, 0$) of the proton structure function, interpolating between the soft (VMD, Pomeron) and hard (GLAP evolution) regimes:

$$F_2^{(S,0)}(x, Q^2) = A \left(\frac{Q^2}{Q^2 + a} \right)^{1+\tilde{\Delta}(Q^2)} e^{\Delta(x, Q^2)}, \quad (3.1)$$

with the "effective power"

$$\tilde{\Delta}(Q^2) = \epsilon + \gamma_1 \ell n \left(1 + \gamma_2 \ell n \left[1 + \frac{Q^2}{Q_0^2} \right] \right), \quad (3.2)$$

and

$$\Delta(x, Q^2) = \left(\tilde{\Delta}(Q^2) \ell n \frac{x_0}{x} \right)^{f(Q^2)}, \quad (3.3)$$

where

$$f(Q^2) = \frac{1}{2} \left(1 + e^{-Q^2/Q_1^2} \right). \quad (3.4)$$

At small and moderate values of Q^2 (to be specified from the fits, see below), the exponent $\tilde{\Delta}(Q^2)$ (3.2) may be interpreted as a Q^2 -dependent "effective Pomeron intercept".

The function $f(Q^2)$ has been introduced in order to provide for the transition from the Regge behavior, where $f(Q^2) = 1$, to the asymptotic solution of the GLAP evolution equation, where $f(Q^2) = 1/2$.

By construction, the model has the following asymptotic limits:

a) Large Q^2 , fixed x :

$$F_2^{(S,0)}(x, Q^2 \rightarrow \infty) \rightarrow A \exp \sqrt{\gamma_1 \ell n \ell n \frac{Q^2}{Q_0^2} \ell n \frac{x_0}{x}}, \quad (3.5)$$

which is the asymptotic solution of the GLAP evolution equation (see Sec. 1).

b) Low Q^2 , fixed x :

$$F_2^{(S,0)}(x, Q^2 \rightarrow 0) \rightarrow A e^{\Delta(x, Q^2 \rightarrow 0)} \left(\frac{Q^2}{a} \right)^{1+\tilde{\Delta}(Q^2 \rightarrow 0)} \quad (3.6)$$

with

$$\tilde{\Delta}(Q^2 \rightarrow 0) \rightarrow \epsilon + \gamma_1 \gamma_2 \left(\frac{Q^2}{Q_0^2} \right) \rightarrow \epsilon, \quad (3.7)$$

$$f(Q^2 \rightarrow 0) \rightarrow 1, \quad (3.8)$$

whence

$$F_2^{(S,0)}(x, Q^2 \rightarrow 0) \rightarrow A \left(\frac{x_0}{x} \right)^\epsilon \left(\frac{Q^2}{a} \right)^{1+\epsilon} \propto (Q^2)^{1+\epsilon} \rightarrow 0, \quad (3.9)$$

as required by gauge invariance.

c) Low x , fixed Q^2 :

$$F_2^{(S,0)}(x \rightarrow 0, Q^2) = A \left(\frac{Q^2}{Q^2 + a} \right)^{1+\tilde{\Delta}(Q^2)} e^{\Delta(x \rightarrow 0, Q^2)}. \quad (3.10)$$

If

$$f(Q^2) \sim 1, \quad (3.11)$$

i.e. when $Q^2 \ll Q_1^2$, we get the standard (Pomeron-dominated) Regge behavior (with a Q^2 dependence in the effective Pomeron intercept)

$$F_2^{(S,0)}(x \rightarrow 0, Q^2) \rightarrow A \left(\frac{Q^2}{Q^2 + a} \right)^{1+\tilde{\Delta}(Q^2)} \left(\frac{x_0}{x} \right)^{\tilde{\Delta}(Q^2)} \propto x^{-\tilde{\Delta}(Q^2)}. \quad (3.12)$$

Within this approximation, the total cross-section for (γ, p) scattering as a function of the center of mass energy W is

$$\sigma_{\gamma,p}^{tot,(0)}(W) = 4\pi^2\alpha \left[\frac{F_2^{(S,0)}(x, Q^2)}{Q^2} \right]_{Q^2 \rightarrow 0} = 4\pi^2\alpha A a^{-1-\epsilon} x_0^\epsilon W^{2\epsilon}. \quad (3.13)$$

4 EXTENSION TO LARGE x

In this section we complete our model by including the large- x domain, extending to $x = 1$, and for all kinematically allowed Q^2 . Since we are essentially concerned with the small- x dynamics (transition between the GLAP and BFKL evolution), the present extension serves merely to have as good fits as possible with a minimal number of extra parameters. To this end we rely on the existing successful phenomenological models, in particular on that of [4a] (CKMT).

Following CKMT, we multiply the singlet part of the above structure function $F_2^{(S,0)}$ (defined in (3.1-3.4)) by a standard large- x factor to get

$$F_2^{(S)}(x, Q^2) = F_2^{(S,0)}(x, Q^2) (1-x)^{n(Q^2)}, \quad (4.1)$$

with

$$n(Q^2) = \frac{3}{2} \left(1 + \frac{Q^2}{Q^2 + c} \right), \quad (4.2)$$

where $c = 3.5489 \text{ GeV}^2$ [4a].

Next we add the nonsinglet (NS) part of the structure function, also borrowed from CKMT

$$F_2^{(NS)}(x, Q^2) = B (1-x)^{n(Q^2)} x^{1-\alpha_r} \left(\frac{Q^2}{Q^2 + b} \right)^{\alpha_r}. \quad (4.3)$$

The free parameters that appear with this addendum are c, B, b and α_r . The final and complete expression for the proton structure function thus becomes

$$F_2(x, Q^2) = F_2^{(S)}(x, Q^2) + F_2^{(NS)}(x, Q^2). \quad (4.4)$$

The total cross-section for (γ, p) scattering is

$$\sigma_{(\gamma,p)}^{tot}(W) = 4\pi^2\alpha \left(A a^{-1-\epsilon} x_0^\epsilon W^{2\epsilon} + B b^{-\alpha_r} W^{2(\alpha_r-1)} \right). \quad (4.5)$$

5 FITTING TO THE DATA

In fitting to the data, the complete experimental "H1" data set (which encloses 237 points: 193 from [15] and 44 from [16]) for the proton structure function $F_2(x, Q^2)$ was used as well as, 76 data points [17] on the (γ, p) total cross-section $\sigma_{(\gamma, p)}^{tot}(W)$.

We note that among a total of 12 parameters, 8 are free, the resting 4 being fixed in the following way:

1. $\epsilon = 0.08$ is a "canonical" value [18], leaving little room for variations (although, in principle, it can be also subject to the fitting procedure);
2. when left free in the fitting procedure, x_0 takes a value slightly beyond 1. Thus, we can safely fix $x_0 = 1$ without practically affecting the resulting fits;
3. as already mentioned, we have set $c = 3.5489 \text{ GeV}^2$ relying on CKMT. This parameter is responsible for the large- x and small- Q^2 region, outside the domain of our present interest;
4. as argued above, we may estimate from QCD the parameter $\gamma_1 = 16N_c(11 - 2f/3)$ with four flavours ($f = 4$) and three colors ($N_c = 3$), it equals 5.76. It corresponds to the asymptotic regime (when $Q^2 \rightarrow \infty$, or $f(Q^2) \rightarrow 1/2$), far away from the region of the fits, where $f = 1$ is more appropriate, hence the value $\gamma_1 = \sqrt{5.76} = 2.4$ is more appropriate in the domain under consideration. Remarkably, this value comes also independently from the fits if γ_1 is let free.

To compare with, the CKMT model [4a] depends on 8 adjustable parameters in the "soft" region, to be completed by QCD evolution at higher values of Q^2 , and with a higher twist term added. On the other hand, the proton structure function and (γ^*, p) cross section in the ALLM model [13,14] are given explicitly in the whole range of the kinematical variables, and the fits to the data are good with a total of 23 adjustable parameters.

When limiting the fitted data to the structure function only [15,16] with $x < 0.1$ (all Q^2), the singlet contribution alone, as approximated in Sec. 3, gives a very good fit ($\chi_{d.o.f}^2 \sim 0.59$), shown in Figs. 1a, 2a. We mention that this result is obtained with an economical set of 8 parameters (5 free), listed in Table 1.

The complete model of Sec. 4 gives very good fits in the whole ranges in x , Q^2 and W covered by measurements. To be specific, we find $\chi_{d.o.f}^2 \sim 0.69$. We show the contributions to the χ^2 of the 3 data sets we used in Table 2, the numerical values for the 12 parameters (8 free) are presented in Table 3.

The results of our fits for the structure function versus Q^2 for fixed x are shown in Fig. 1 b and for fixed Q^2 as a function of x are in Figs. 2b, 3. The total cross section for real photons on protons as function of W is displayed in Fig. 4.

6 INTERFACE BETWEEN SOFT AND HARD DYNAMICS AND TRANSITION FROM BFKL TO GLAP EVOLUTION

6.1 $\frac{\partial F_2}{\partial(\ln Q^2)}$ as a function of x and Q^2 .

The derivative of the SF with respect to $\ln Q^2$ (slope for brevity) measures the amount of the scaling violation and eventually shows the transition from soft to hard dynamics. This derivative depends on two variables (x and Q^2). It was recently calculated from the HERA data [3]; in Figs. 5, 6a we have quoted the corresponding results. In those calculations the variables x and Q^2 are strongly correlated, it is implied that, for a limited acceptance (as it is the case in the HERA experiments) and for a fixed energy, one always has a limited band in Q^2 at any given x , with average Q^2 becoming smaller for smaller x . From a theoretical point of view, however, x and Q^2 are quite independent and one is not restricted to follow a particular path on the surface representing the slope. Therefore we plot in Fig. 5 the slope calculated

from our model (4.4) with the parameters fitted to the data, in one more dimension than usual, *i.e.* as a function of the two independent variables - x and Q^2 . The two slopes on the hill of $\frac{\partial F_2}{\partial(\ln Q^2)}$ in Fig. 5 correspond to soft and hard dynamics. The division line is only symbolic since there is a wide interface region where both dynamics mix, each tending to dominate on the lower side of its own slope. Remarkably, the division line - or line of maxima of this surface - turns out to be almost Q^2 -independent ($\sim 40 \text{ GeV}^2$). The difference with the maximum at 2 GeV^2 exhibited in [3] is due to the special experimental set of (x, Q^2) chosen in [3], discussed above and shown in Fig. 5.

Notice that the slope becomes negative in a region between $Q^2 \sim 200$ and $\sim 4000 \text{ GeV}^2$, at small x ; this region tends to narrow when x increases beyond $x = 0.0005$ and finally disappears when x exceeds 0.05.

The same results are exposed on families of 2-dimensional figures as well (Figs. 6a, 6b) showing the x - (and Q^2 -) dependence of the slope when the other variable takes fixed values. Fig. 6a shows that our predictions are quite in agreement with the data from [3]; also shown is the failure of the approach of the GLAP evolution equation [12] to follow the low x (Q^2) dynamics as reported in [3]. Fig. 6b shows the variation with x of the region with negative slope. Notice that the rising part to large extent is a threshold effect due to the increasing phase space (see [19]).

6.2 $\frac{\partial \ln F_2}{\partial(\ln(1/x))}$ as a function of Q^2 for some x values.

The derivative of the logarithm of the SF with respect to $\ln 1/x$, when measured in the Regge region, can be related (for low x) to the Pomeron intercept. In Fig. 7 the Q^2 -dependence of this derivative is shown for some low x - values, together with the "effective power" $\tilde{\Delta}$ (3.2). On the same figure, the behavior of the function $f(Q^2)$ (3.4) is also shown. In our model, Regge behavior is equivalent to the condition that $f(Q^2)$ is close to unity. This lower limit, marked on Fig. 7 (tentatively approximated within a 2 % accuracy for the function $f(Q^2)$), is located near 40 GeV^2 . Until this landmark, the effective power $\tilde{\Delta}$ indeed remains very close to $\frac{\partial \ln F_2}{\partial(\ln(1/x))}$, beyond Regge behavior is not valid (since $f \neq 1$) and $\tilde{\Delta}$ cannot be considered as the effective slope any more. On the other hand, $\frac{\partial \ln F_2}{\partial(\ln(1/x))}$ turns down as Q^2 increases, approaching its "initial value" of ≈ 0.1 at largest Q^2 and coming closer to the unitarity bound. Notably, at large Q^2 the derivative gets smaller as x decreases, contrary to the general belief that dynamics becomes harder for smaller x , but in accord with an observation made in [20]. Care should be however taken in interpreting the "hardness" of the effective power outside the Regge region.

According to our model, the change from the BFKL (Pomeron) to the GLAP evolution occurs when $f(Q^2)$ changes from 1 to $1/2$. This variation happens in a band in Q^2 , namely between $\sim 40 \text{ GeV}^2$ and $\sim 4000 \text{ GeV}^2$.

Let us remind once more that our interpolating formula (3.1) between Regge behavior and GLAP evolution was suggested for small x ($x \leq 0.1$). The larger x part was introduced for completeness and better fits only, without any care of its correspondence to the GLAP evolution equation. It does not affect however the kinematical domain of the present and future HERA measurements and Pomeron dominance (BFKL evolution) we are interested in.

7 CONCLUSIONS

Once the "boundary conditions" (at low and high Q^2) are satisfied, the interpolation may be considered as an approximate solution valid for all Q^2 . Clearly, our interpolation is not unique. For example, the choice of $f(Q^2)$, satisfying the boundary conditions $f(0) = 1$ and $f(\infty) = 1/2$, may be different from ours. However, there is little freedom in the choice of the

asymptotic forms, different from those we have used, namely (3.5) and (3.12). The utilization of a soft Pomeron input different from (3.12) is credible. For example, a dipole Pomeron was shown [7, 11] to have the required formal properties and to fit the data at small and moderate Q^2 . Moreover, the dipole Pomeron does not violate the Froissart bound, so it does not need to be unitarized. Attempts [6, 7] to fit the high- Q^2 HERA data without a power in x , i.e. with logarithmic functions, attributing the whole Q^2 dependence to the (factorized) "residue function", are disputable. What is even more important from the point of view of the present interpolation, a power in x must be introduced anyway to match the high Q^2 GLAP evolution solution (3.5). This discussion brings us back to the interesting but complicated problem of unitarity.

As it is well known, the power increase of the total cross sections, or of the SF towards small x cannot continue indefinitely. It will be slowed down by unitarity, or shadowing corrections, whose calculation or even recipe - especially for high virtualities Q^2 - is a delicate and complicated problem, beyond the scope of the present paper. Here we only mention, that once the model fits the data, it cannot be far from the "unitarized" one in the fitted range, since the data "obey" unitarity.

To conclude:

1. Strong interaction dynamics is continuous, hence the relevant solutions should be described by continuous solutions as well;
2. The formal solutions of the GLAP equations, even in their most advanced forms, ultimately contain some freedom (e.g. "higher twists", or non-perturbative corrections) or approximations;
3. However so elaborated or "precise" the existing solutions are, unitarity corrections will modify their form anyway;

The above remarks justify the use for practical purposes of an explicit solution that satisfies the formal theoretical requirements and yet fits the data. Its simplicity and flexibility make possible its further improvement and its use as a laboratory in studying complicated and yet little understood transition phenomena.

ACKNOWLEDGEMENTS

We thank M. Bertini for discussions and L.A. Bauerdick for a useful correspondence.

References

- [1] V. N. Gribov, L. N. Lipatov, Sov. J. Nucl. Phys. **15**, 438 and 675 (1972); G. Altarelli, G. Parisi, Nucl. Phys. B **126**, 298 (1977).
- [2] Y. Y. Balitskii, L. N. Lipatov, Sov. Physics JETP **28**, 822 (1978); E. A. Kuraev, L. N. Lipatov, V. S. Fadin, ibid. **45**, 199 (1977); L. N. Lipatov, ibid. **63**, 904 (1986).
- [3] L. Bauerdick, *Proton structure function and (γ^*, p) cross section at HERA in Interplay between Hard and Soft Interactions in Deep Inelastic Scattering, Max Planck workshop, Heidelberg, 1997* (transparencies available from: <http://www.mpi-hd.mpg.de/hd97/>).
- [4] a) A. Capella, A. Kaidalov, C. Merino, J. Tran Thanh Van, Phys. Lett. B **337**, 358 (1994).
b) M. Bertini, P. Desgrolard, M. Giffon, E. Predazzi, Phys. Lett. B **349**, 561 (1995).
- [5] A. Capella, A. Kaidalov, V. Neichitailo, J. Tran Thanh Van, LPTHE-ORSAY 97-58 and hep-ph/9712327, 1997.
- [6] W. Buchmuller, D. Haidt, DESY/96-61, 1996.
- [7] L. L. Jenkovszky, E. S. Martynov, F. Paccanoni, *Regge behavior of the nucleon structure functions*, PFPD 95/TH/21, 1995; L. L. Jenkovszky, A. Lengyel and F. Paccanoni, *Parametrizing the proton structure function*, hep-ph/9802316, 1998.
- [8] R. D. Ball, S. Forte. Phys. Lett. B **335**, 77 (1994); F. Paccanoni, *Note on the DGLAP evolution equation*, in **Strong Interaction at Long Distances**, edited by L. L. Jenkovszky (Hadronic Press, Palm Harbor, 1995).
- [9] M. Bertini, M. Giffon, L. L. Jenkovszky, F. Paccanoni, E. Predazzi, Rivista Nuovo Cim. **19**, 1 (1996).
- [10] V. S. Fadin, L. N. Lipatov, *BFKL Pomeron in the next-to-leading approximation*, hep-ph/9802290, 1998.
- [11] L. L. Jenkovszky, A. V. Kotikov, F. Paccanoni, Phys. Lett. B **314**, 421 (1993).
- [12] M. Glück, E. Reya, A. Vogt. Zeit. Phys. C **67**, 433 (1995).
- [13] H. Abramowicz, E. Levin, A. Levy, U. Maor, Phys. Lett. B **269**, 465 (1991).
- [14] H. Abramowicz, A. Levy, DESY 97-251 and hep-ph/9712415, 1997.
- [15] S. Aid *et al.* H1 collaboration, Nucl. Phys. B **470**, 3 (1996):
193 values of the structure function of the proton, for Q^2 , between 1.5 GeV² and 5000 GeV², and x , between $3 \cdot 10^{-5}$ to 0.32 (of which 169 data correspond to $x < 0.1$).
- [16] C. Adloff *et al.* H1 collaboration, Nucl. Phys. B **497**, 3 (1997):
44 values of the structure function of the proton, at low x , down to $6 \cdot 10^{-6}$, and low Q^2 , between 0.35 GeV² and 3.5 GeV².
- [17] D.O. Caldwell *et al.*, Phys. Rev. D **7**, 1384 (1975); Phys. Rev. Lett. **40**, 1222 (1978).
M. Derrick *et al.* ZEUS collaboration, Zeit. Phys. C **63**, 391 (1994).
S. Aid *et al.* H1 collaboration, Zeit. Phys. C **69**, 27 (1995).
- [18] H. Cheng, J.K. Walker, T.T. Wu, Phys. Lett. B **44**, 97 (1973);
A. Donnachie, P.V. Landshoff, Phys. Lett. B **296**, 493 (1975).
- [19] L. L. Jenkovszky, E. S. Martynov, F. Paccanoni, Nuovo Cimento A **110**, 649 (1997).
- [20] A. De Roeck, E. A. De Wolf, Phys. Lett. B **388**, 188 (1996).

Tables captions

Table 1.

Parameters used in our "first approximation fit" ($x < 0.1$).

Table 2.

χ^2 - contributions of each set of data used in our fit with the parameters listed in Table 3.

Table 3.

Parameters used in our fit in the whole kinematical range (see the text).

Figures captions

Fig. 1 a Proton structure function $F_2(x, Q^2)$ as a function of Q^2 at various values of fixed x . For a better display, the structure function values have been scaled at each x by the factor shown in brackets on the same line as the x values. The shown H1 - data are from [15,16], the error bars represent the statistical and systematic errors added in quadrature, the curves are the results of our first parametrization fitted on $x < 0.1$ data ("low- x , Pomeron dominated" approximation, the parameters being listed in Table 1).

Fig. 1 b Proton structure function $F_2(x, Q^2)$ as a function of Q^2 at various values of fixed x as in Fig. 1 a but the curves being the results of our second parametrization fitted to all H1 data [15,16] of the proton structure function and to the total cross-sections of the (γ, p) process [17] (the parameters are listed in Table 3).

Fig. 2 a Proton structure function $F_2(x, Q^2)$ as a function of x at various values of fixed Q^2 . Results of our first approximation, see also Fig. 1 a.

Fig. 2 b Proton structure function $F_2(x, Q^2)$ as a function of x at various values of fixed Q^2 . Results of our second parametrization, see also Fig. 1 b.

Fig. 3 Proton structure function $F_2(x, Q^2)$ as a function of x at various low Q^2 values. See also Fig. 1 b.

Fig. 4 Total cross-section of the reaction (γ, p) $\sigma_{(\gamma, p)}^{tot}$ as a function of W , center of mass energy. (see also Fig. 1 b).

Fig. 5 Two-dimensional projection of the three dimensional "slope" of the proton structure function. The surface represents $\frac{\partial F_2(x, Q^2)}{\partial(\ln Q^2)}$ as a function of x and Q^2 as following from the present parametrization with its line of maximum (open squares). The crosses are the points calculated from the HERA data in [3], located on an experimental (x, Q^2) path.

Fig. 6a Derivative of the proton structure function $\frac{\partial F_2(x, Q^2)}{\partial(\ln Q^2)}$ as a function of x , for some Q^2 values as indicated. The round dots are the HERA data, the open squares the results from [12] taken from [3] and the hollow triangles are the results of the present parametrization.

Fig. 6b Same derivative as in Fig. 6a $\frac{\partial F_2(x, Q^2)}{\partial(\ln Q^2)}$ as a function of Q^2 , for some x values as indicated. The solid curves are the results of the present parametrization.

Fig. 7 Derivative of the logarithm of the proton structure function $\frac{\partial \ln F_2(x, Q^2)}{\partial(\ln(1/x))}$ versus Q^2 for some x values as indicated. Also plotted on the same (left) scale is the effective exponent $\tilde{\Delta}$ (3.2), representing the Pomeron intercept -1 . only when $f(Q^2) \approx 1$. The function $f(Q^2)$ (3.4) is also shown as a dashed line (right scale); the transition between the Regge behavior ($f = 1$.) and the GLAP evolution ($f = 0.5$) occurs within an estimated band located between vertical landmarks (see the text).

A	0.1612
a (GeV) ²	0.2133
γ_2	0.02086
Q₀² (GeV) ²	0.2502
Q₁² (GeV) ²	676.9
x₀	1.0 (fixed)
ϵ	0.08 (fixed [18])
γ_1	2.4 (fixed QCD)

Table 1.

Parameters used in our "first approximation fit" ($x < 0.1$).

Data set	N. of points	χ^2
$\sigma_{(\gamma,p)}^{tot} (W > 3 \text{ GeV}^2)$ [17]	73	73
$F_2, \text{ H1}$ [15]	193	116
$F_2, \text{ H1 (low } x)$ [16]	44	20

Table 2.

χ^2 - contributions of each set of data used in our fit with the parameters listed in Table 3.

A	0.1623
a (GeV) ²	0.2919
γ_2	0.01936
Q₀² (GeV) ²	0.1887
Q₁² (GeV) ²	916.1
B	0.3079
b (GeV) ²	0.06716
α_r	0.5135
x₀	1.0 (fixed)
ϵ	0.08 (fixed [18])
γ_1	2.4(fixed QCD)
c (GeV) ²	3.549 (fixed [4a])

Table 3.

Parameters used in our fit in the whole kinematical range (see the text).

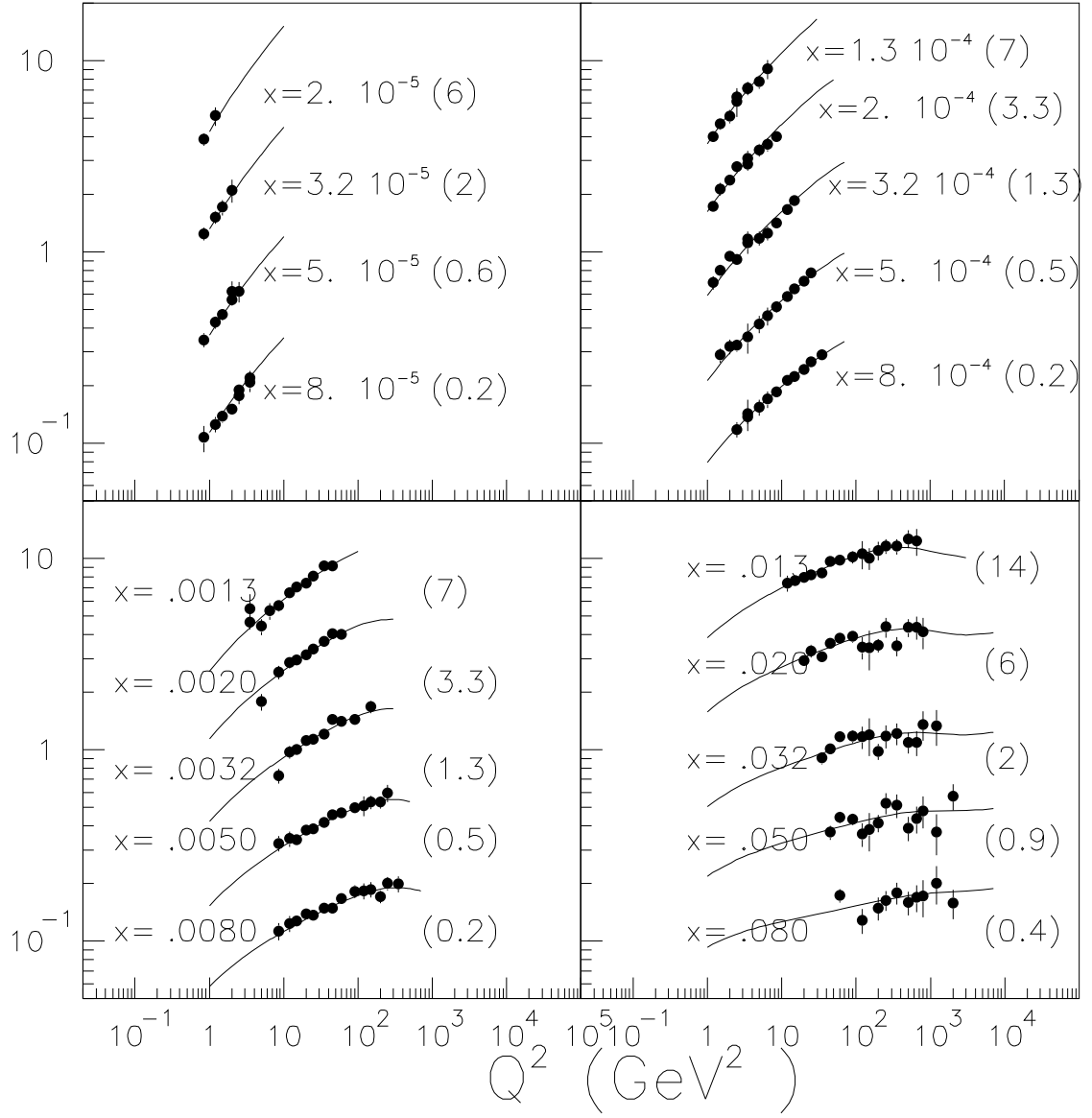


Fig. 1a

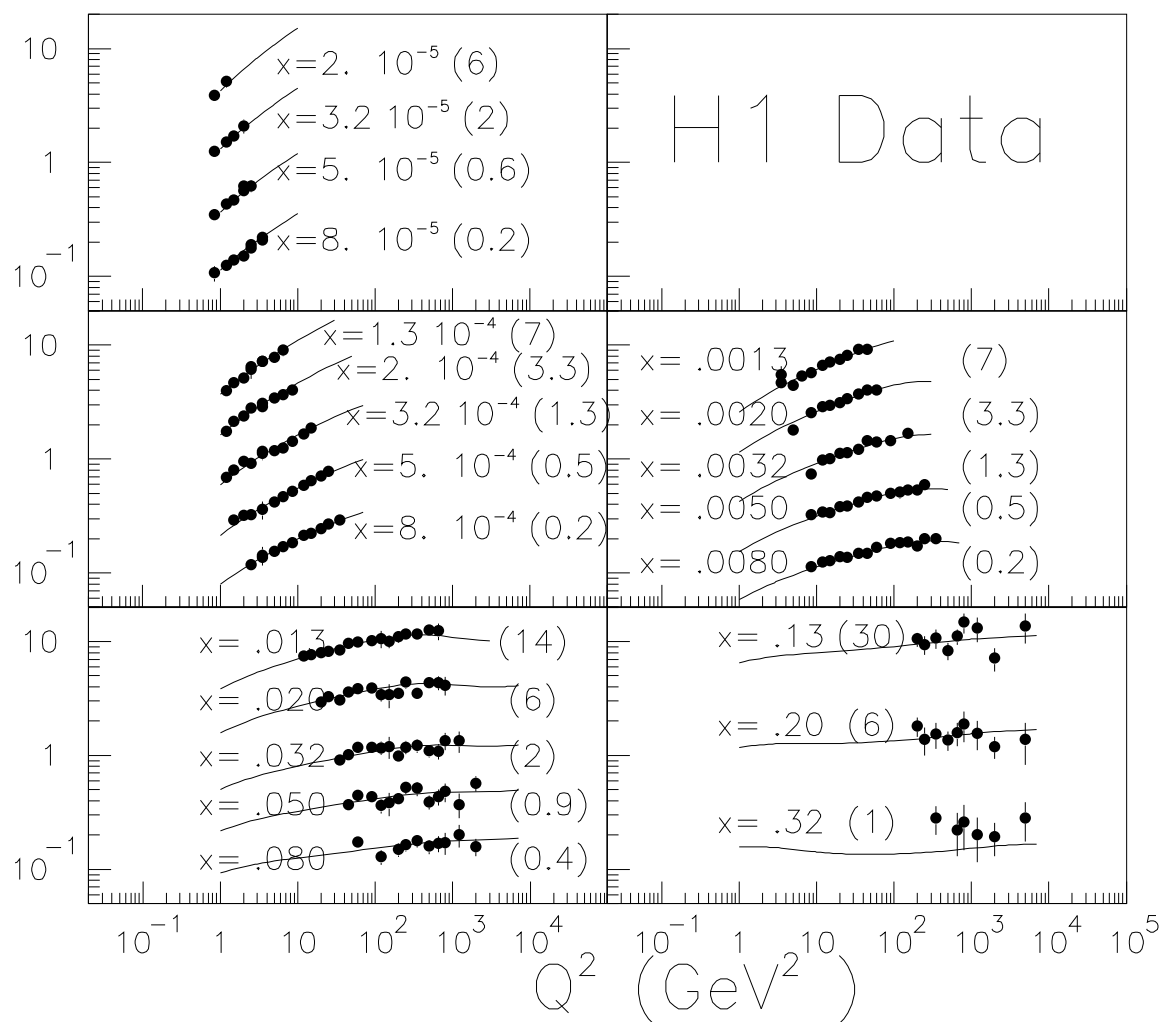


Fig. 1b

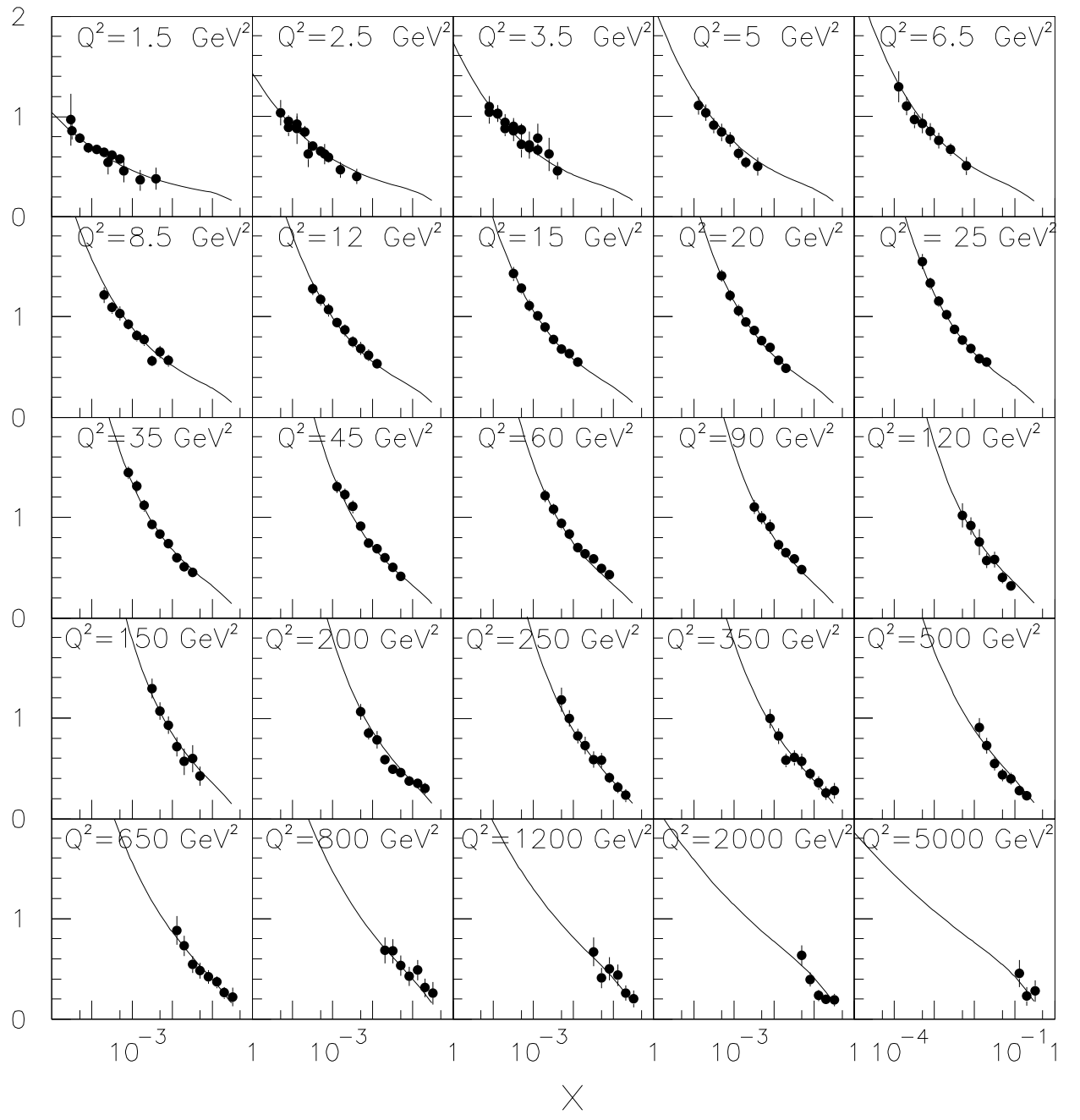


Fig. 2a

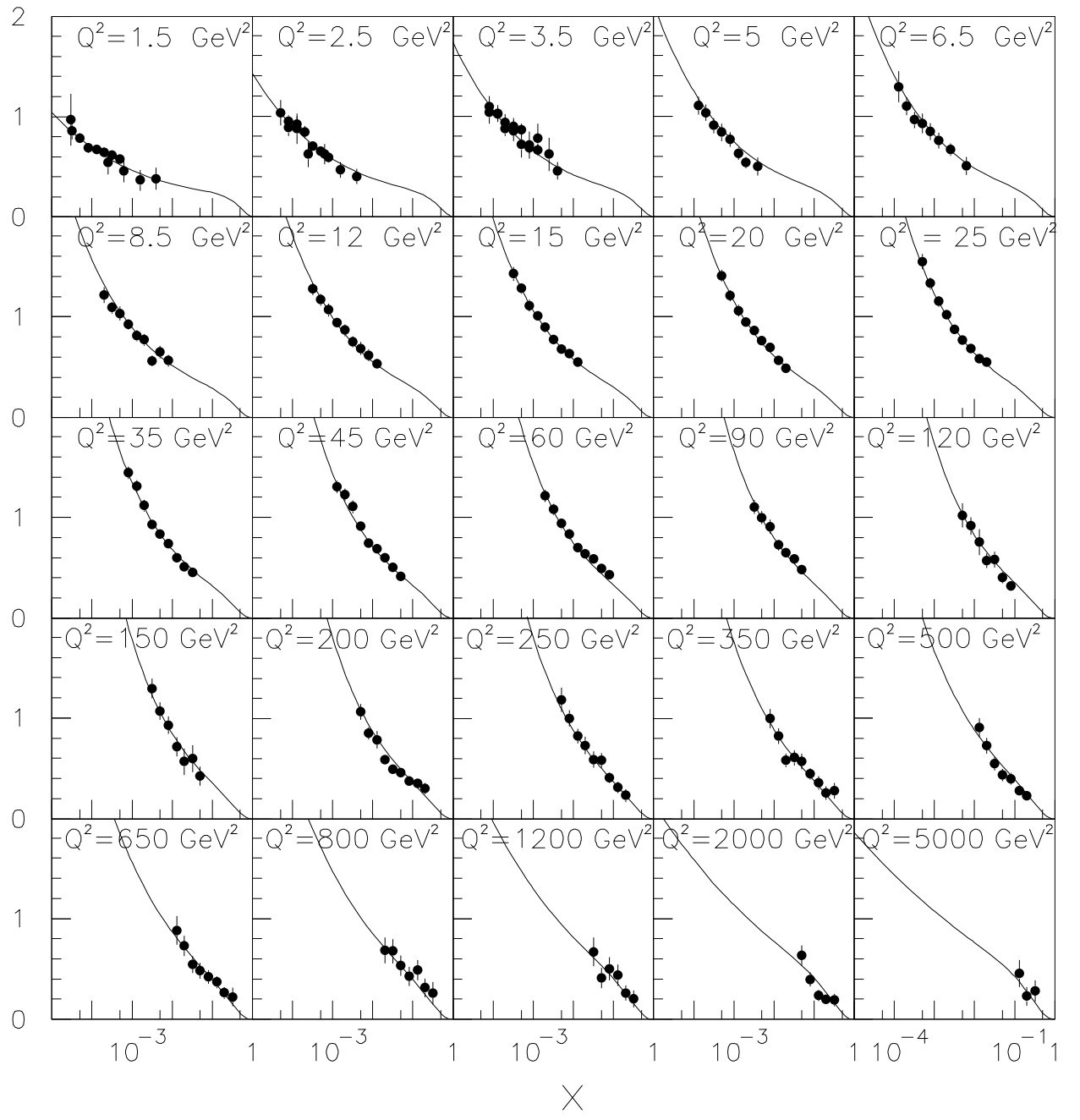


Fig. 2b

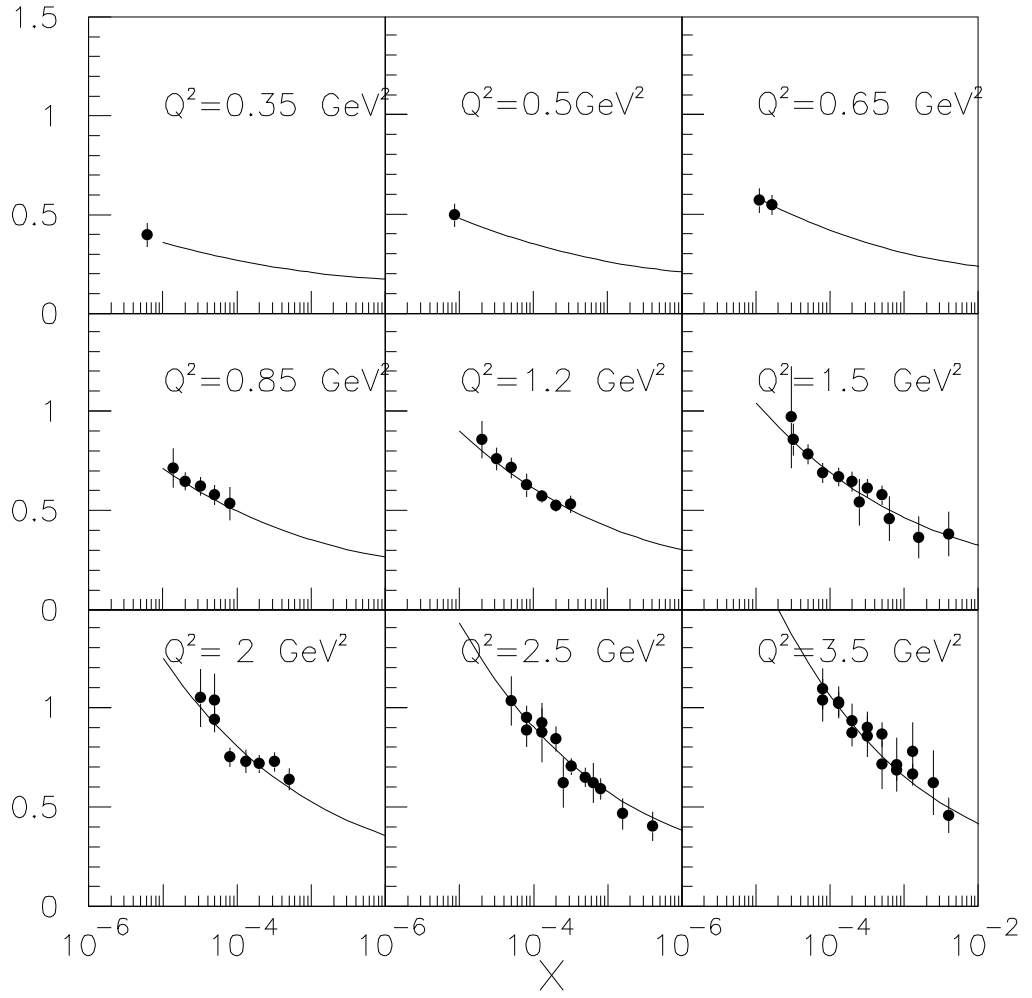


Fig. 3

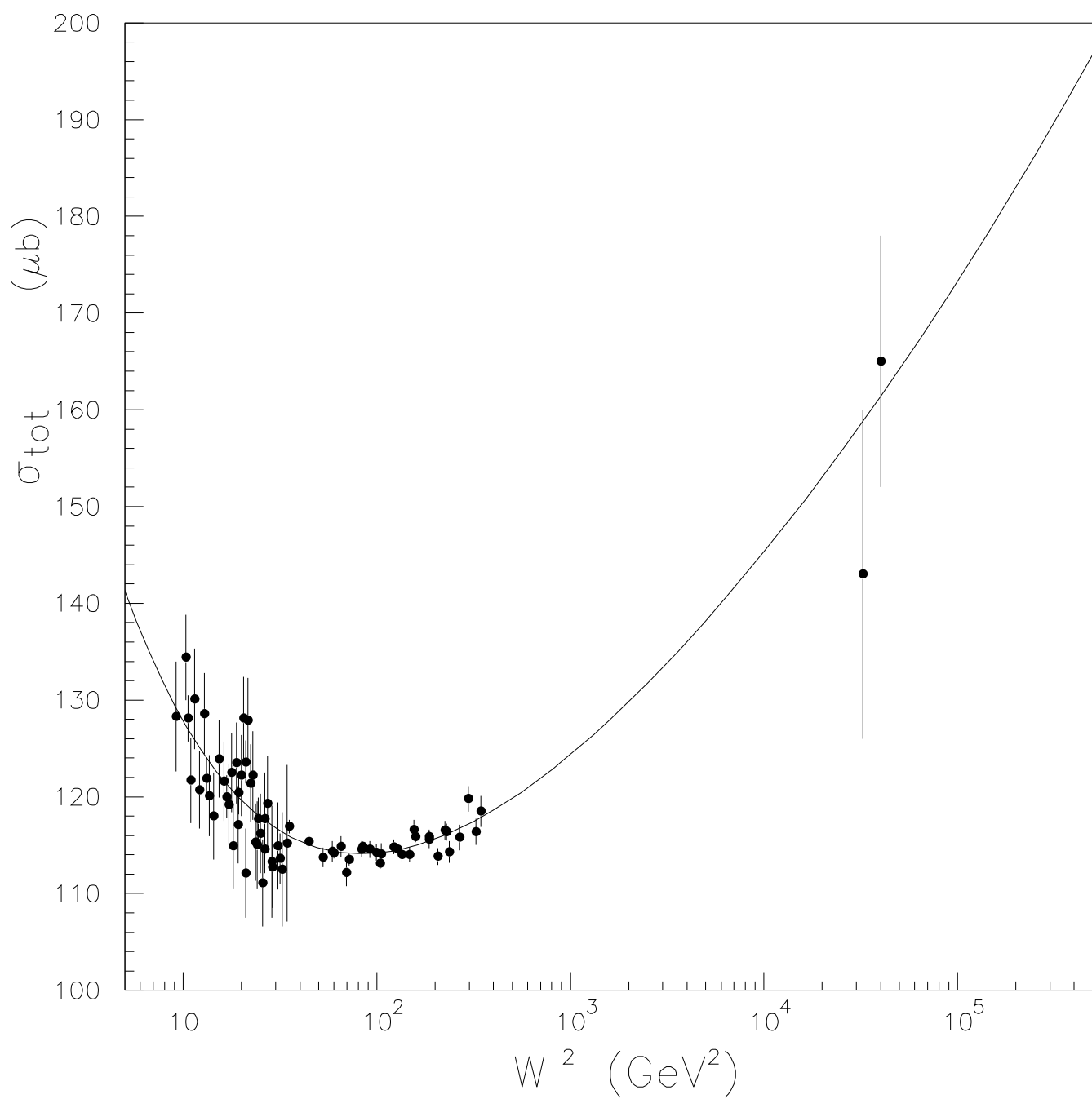


Fig. 4

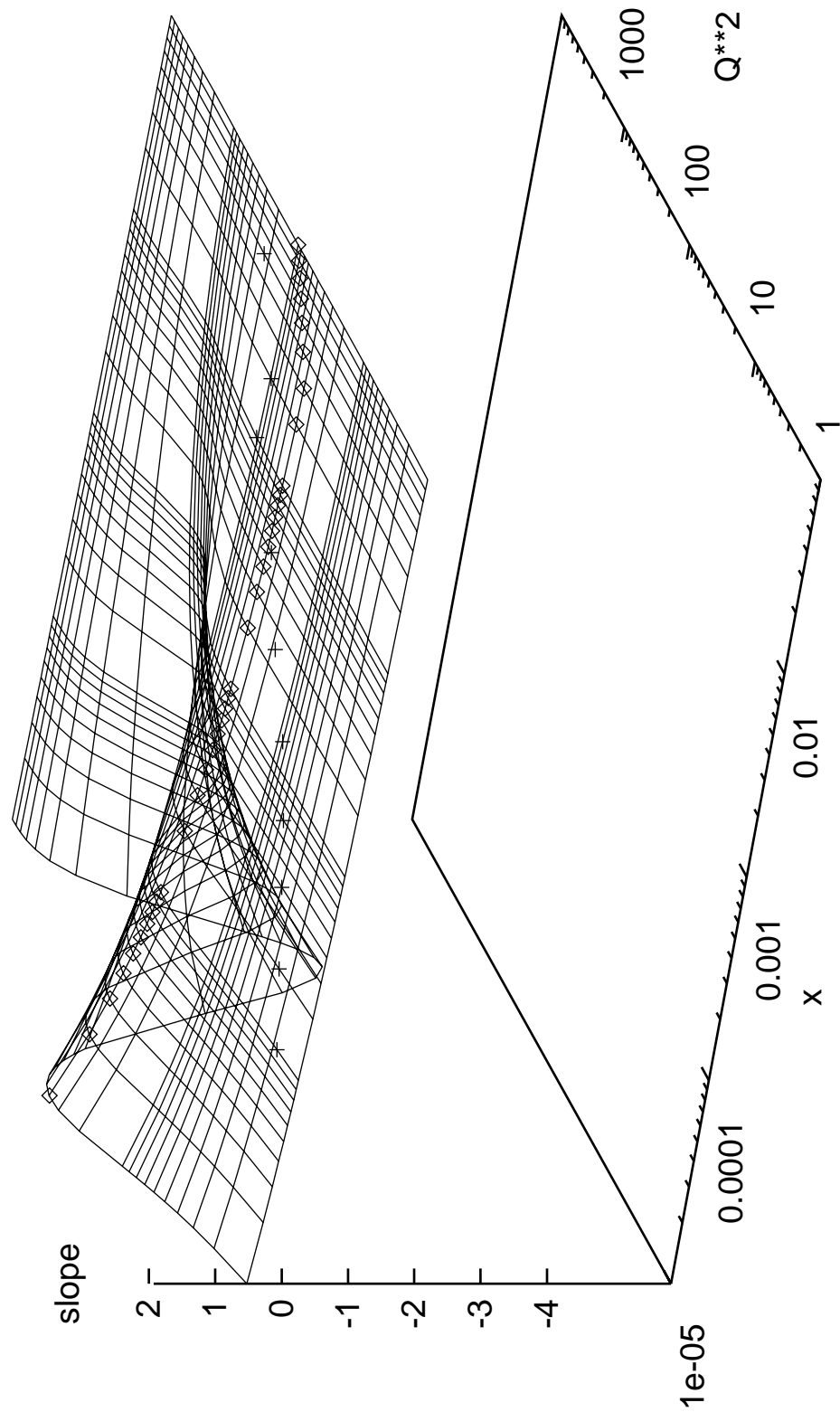


Fig. 5

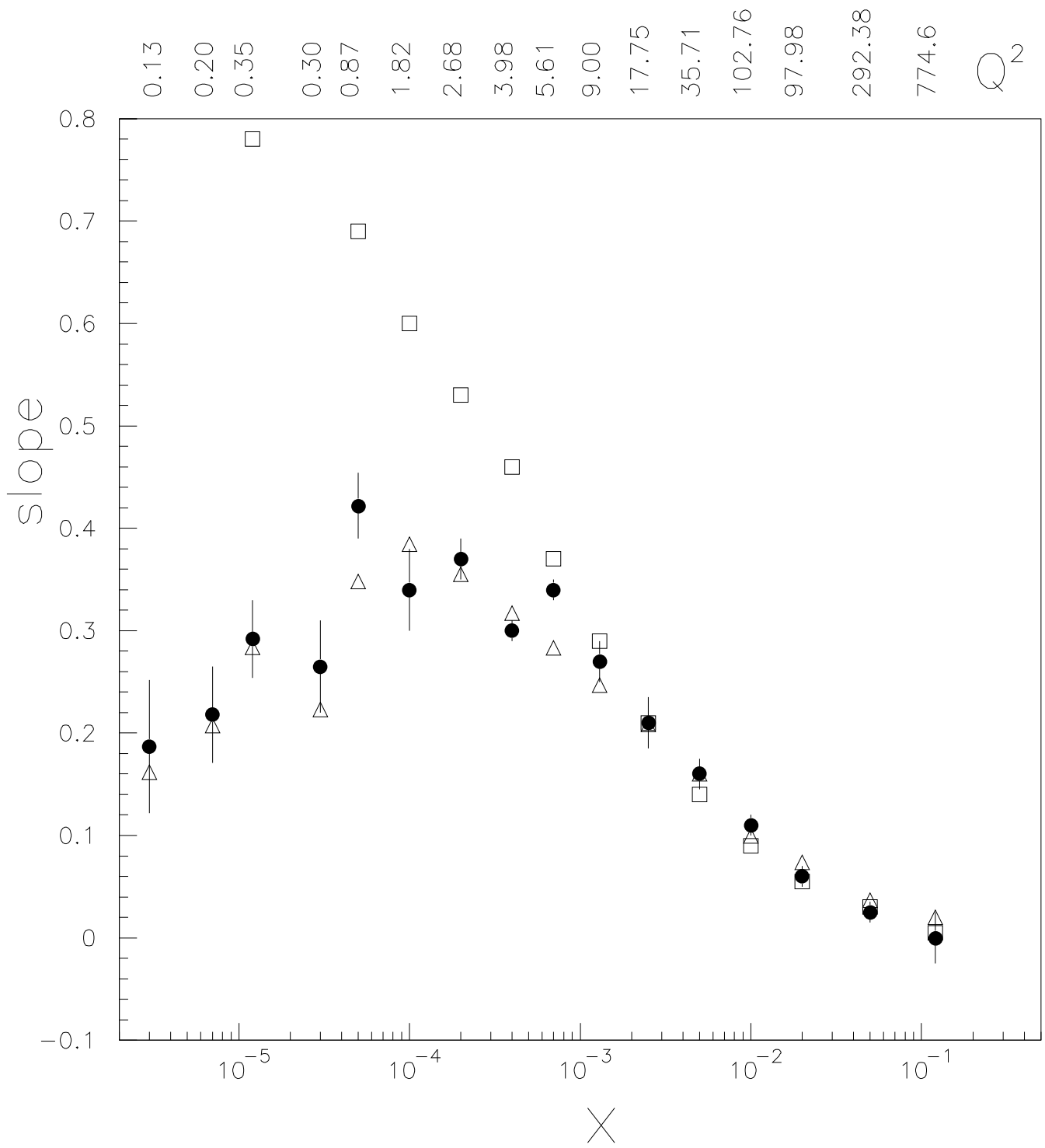


Fig. 6a

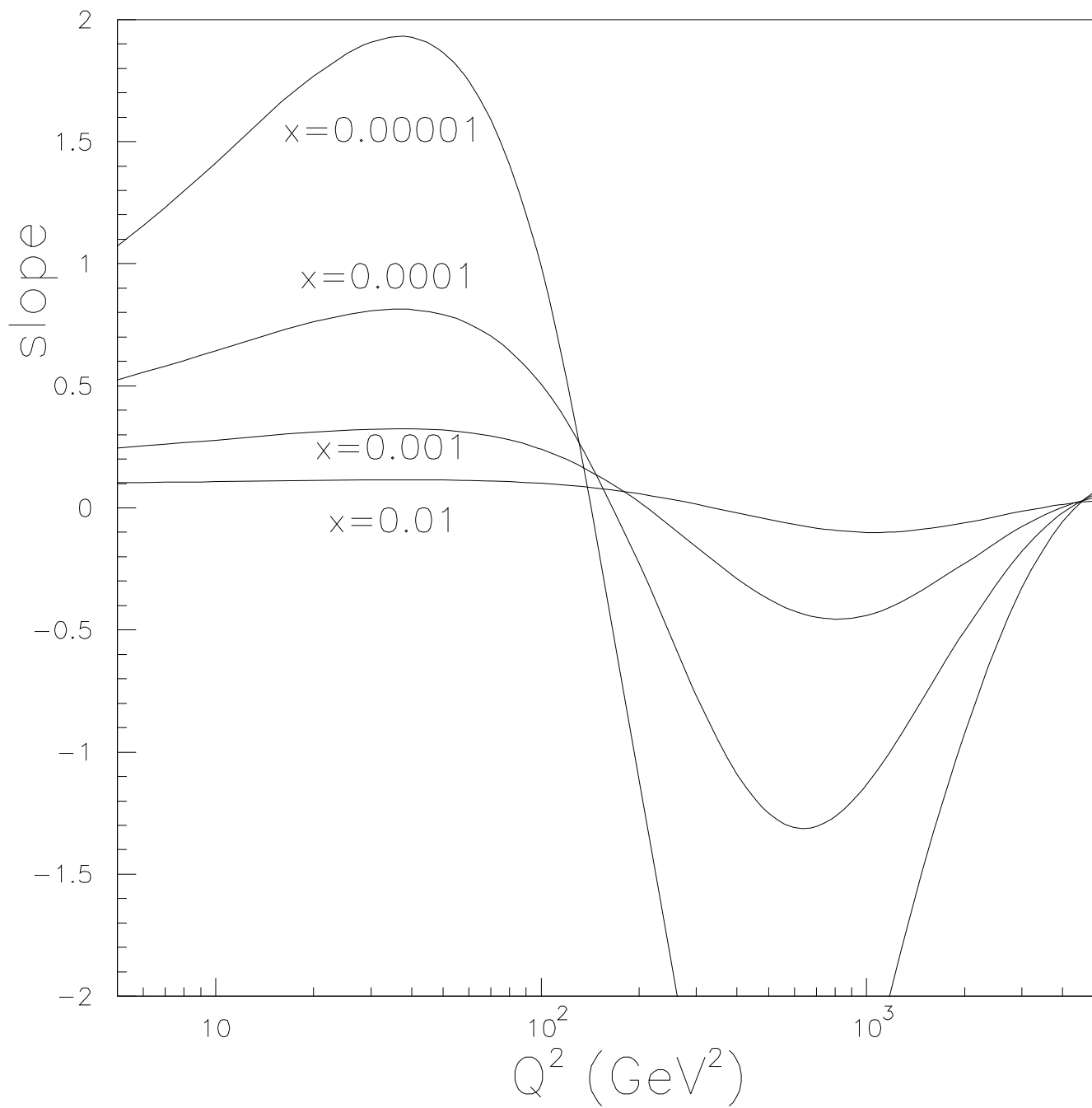


Fig. 6b

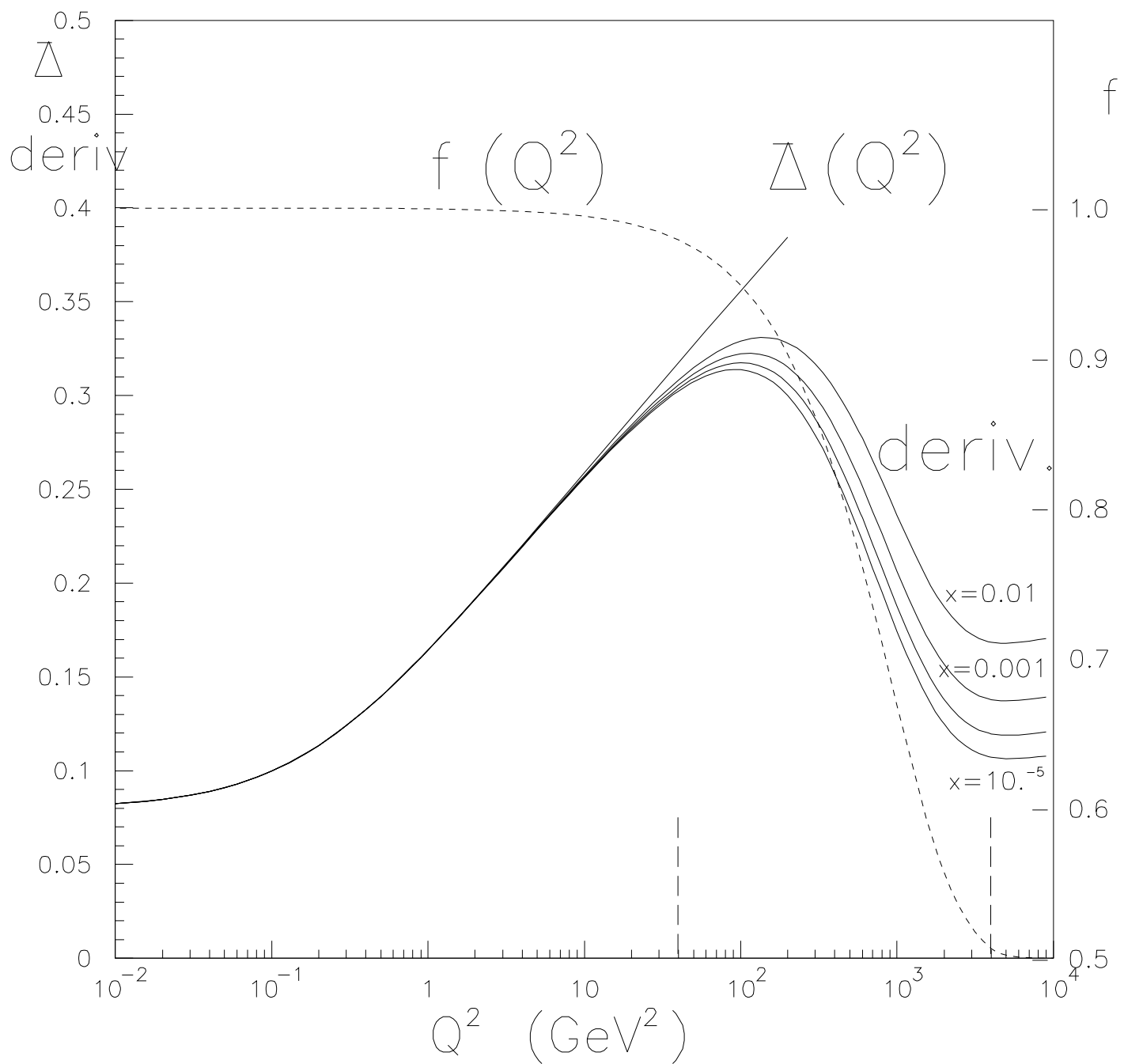


Fig. 7